MEASUREMENT OF THE TIME-STRUCTURE OF THE 72 MEV PROTON BEAM IN THE PSI INJECTOR-2 CYCLOTRON

R. Dölling, Paul Scherrer Institut, Villigen, Switzerland

Abstract

The time-structure monitor at the last turn of the 72 MeV Injector-2 cyclotron has been improved in order to meet the stringent time-resolution requirement imposed by the short bunch length. Protons scattered by a thin carbon-fibre target pass through a first scintillator-photomultiplier detector and are stopped in a second one. The longitudinal bunch shape is given by the distribution of arrival times measured with respect to the 50 MHz reference signal from the acceleration cavities. From a coincidence measurement, the time resolution of the detectors has been determined to be 51 ps and 31 ps fwhm. Longitudinal and horizontal bunch shapes have been measured at beam currents from 25 μA to 1700 μA. Approximately circular bunches were observed with diameter increasing with current. The shortest observed proton bunch length was 38 ps fwhm.

1 INTRODUCTION

Time-structure measurement has been used at PSI since 1974 and has delivered valuable information during the commissioning of Injector 2 and at the introduction of the buncher in the injection line to Injector 2 [1 - 6]. Due to the buncher, the bunch length inside the cyclotron was reduced from ~15° fwhm of RF period to below 5° and it was not clear if the resolution of the time-structure monitor was still sufficient to resolve the bunch shape. In the end of 2000 a new double detector set-up based on NE111 scintillators and Hamamatsu R7400 metal package PMTs with custom divider circuits was tested, which allowed for the determination of the time resolution.

2 EXPERIMENTAL SET-UP

The monitor is located half a turn in front of the beam extraction in the space between two sector magnets. A carbon fibre of 30 μm diameter is moved transversally through the beam by a motorised feedthrough (Fig. 1). The detectors are located above, behind a 0.5 mm stainless steel window and a stainless steel aperture of 4.5 mm diameter. Scintillator A (a 8x8x16 mm^3 piece of NE111) is separated from scintillator B (8x8x40 mm^3 from the same piece of raw material) by a 12 μm aluminium foil which also covers the surface opposite to PMT A in order to enhance light collection. Both PMTs are coupled to the scintillators by silicon grease.

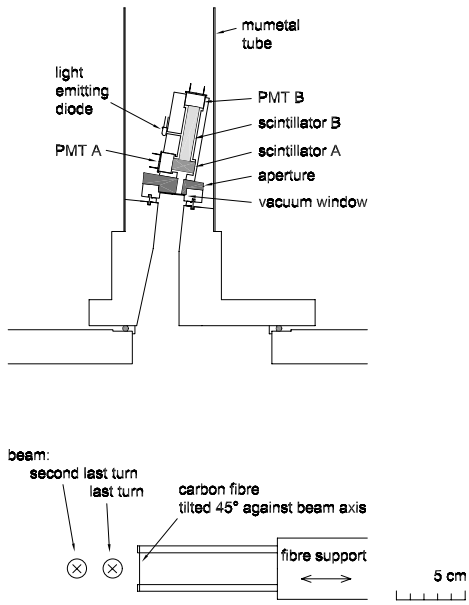

Fig. 1: Detector geometry.

An overview of the electronic set-up and modes of operation is given in Fig. 2. The output signals from the PMTs are transmitted through approximately 80 m of 50 Ω Cellflex LCF ½" cable to the control room. After passing an ohmic divider, one part of the signal is fed to an Elscint STD-N-1 snap-off timing discriminator (SOD) [7] and the other part is used for pulse height discrimination. Besides the elastically scattered protons, there are protons with lower energy from inelastic scattering at the carbon fibre and from scattering at the aperture, which arrive later. Hence, only the highest pulses at PMT B correspond to the correct timing information, and pulse height discrimination is necessary. This is provided by a SIN-FDD100 leading edge discriminator (LED). For a time-structure measurement with PMT B, the fast timing signal of SOD B is allowed to proceed as the start signal to a Canberra 2043 time-to-amplitude converter (TAC) if the pulse height of PMT B surpasses a defined high level. Gating is provided by a SIN-FC107B logic module. The stop signal is derived from the 50 MHz RF-reference signal by a SIN ZCD100A zero-crossing detector and gated in the same way. If the probe is positioned at the centre of a 1600 μA beam, the rate of accepted pulses is of the order of 250 cps.

If the time structure is measured with PMT A, pulse height discrimination is done also with the PMT B signal.

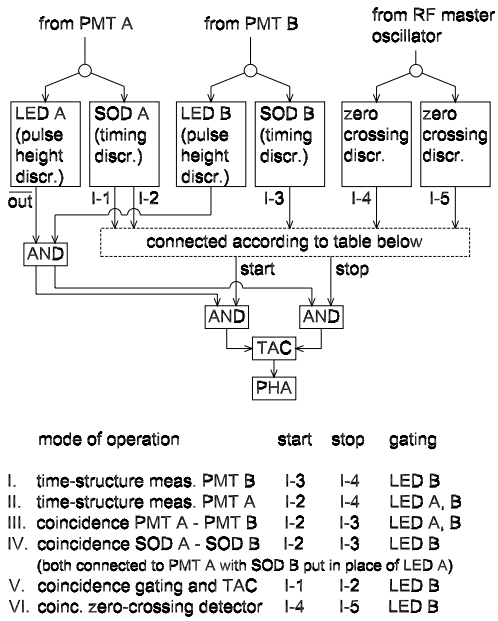

Fig. 2: Block diagram of the timing system.

The TAC-output is connected to a Northern-Econ-2 pulse height analyser (PHA). The overall conversion gain was determined to be 8.7 ps/channel by introducing known delays. Usually, the fwhm and full-width-20%-maximum values of the time spectra were recorded, and its ratios corresponded well with a gaussian shape of the spectra. All times given below are fwhm.

Time structure as well as coincidence measurements were performed with the carbon fibre positioned near the centre of the beam. Transversal beam profiles were determined by measuring the rate of accepted pulses at several beam positions.

3 RESULTS AND DISCUSSION

3.1 Non-linearity of pulse height and charge

The height and shape of the highest PMT output pulses, corresponding to elastically scattered protons, were measured with a fast oscilloscope. The dependency of pulse height and pulse charge Q_{pulse} on the PMT supply voltage U_{PMT} is given in Fig. 3. The non-linear behaviour at higher supply voltages can probably be attributed to space-charge forces resulting from the high pulse current density at the last dynodes. No dependency of pulse height on pulse rate was observed.

3.2 Estimation of the number of photoelectrons

The gain of the individual PMT is determined from the ratio of anode and cathode luminous sensitivities provided by the manufacturer. The quantities of photoelectrons generated at the photocathodes of the individual PMTs 1 and 2 at positions A and B in response to elastically scattered protons were determined according to Fig. 3. This was repeated after interchanging the PMTs (Table 1). The higher numbers with PMT 2 reflect its higher quantum efficiency.

Table 1: Quantities of generated photoelectrons.

	PMT 1	**PMT 2**
serial number	AD7126	AD7266
cathode lumin. sens.* [μA/lm] [9]	56.9	65.6
anode luminous sens.* [A/lm] [9]	33.3	21.2
individual gain*	585000	323000
N_{PE} at position A	1927	2173
N_{PE} at position B	4900	5500

* at U_{PMT} = -800 V

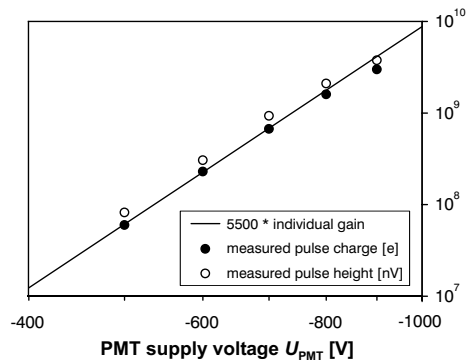

Fig. 3: Pulse height and charge of output pulses of PMT 2 at position B. The straight line represents the dependency of the gain on the supply voltage for this type of PMT [8] normalized to the gain of the individual tube (Table 1) and fitted by a factor (5500) to the measured pulse charge at lower supply voltages. This factor corresponds to the number of photoelectrons N_{PE} generated at the photocathode: $N_{PE} = Q_{pulse} / (e * gain)$ with e the electron charge.

3.3 Estimation of time resolution

The time resolution of detectors A and B can be deduced from the width t_{AvsB} = 60 ps of the coincidence spectrum measured according to Fig. 2, mode III. From the separation

$$t_{AvsB}^2 = t_{loc,A}^2 + t_{det,A}^2 + t_{det,B}^2 + t_{elo}^2 \quad (1)$$

$t_{det,A}$, $t_{det,B}$ the time jitter of the detectors (scintillator and PMT) at positions A and B

$t_{loc,A}$ = 16 ps the time jitter introduced by the variety of distances between individual proton paths and PMT A which is allowed by the aperture

t_{elo} = 21 ps the time jitter of the electronics measured according to Fig. 2, modes IV, V, VI

and the known fact that the time jitter of the detectors scales with the inverse square root of the number of photoelectrons generated at the photocathode [10, 11]

$$t_{det,A}^2 / t_{det,B}^2 = N_{PE,B} / N_{PE,A} \quad (2)$$

follows with $N_{PE,A}$, $N_{PE,B}$ from Table 1 (PMT 1 at position A, PMT 2 at position B)

$$t_{\mathrm{det,B}} = \sqrt{\frac{t_{\mathrm{AvsB}}^2 - t_{\mathrm{loc,A}}^2 - t_{\mathrm{elo}}^2}{1 + N_{\mathrm{PE,B}}/N_{\mathrm{PE,A}}}} = 27\,\mathrm{ps} \qquad (3)$$

$$t_{\mathrm{det,A}} = 46\,\mathrm{ps}$$

as well as the time jitter of the detectors including the contribution of electronic jitter and path variety

$$t_{\mathrm{total,B}} = \sqrt{t_{\mathrm{det,B}}^2 + t_{\mathrm{elo}}^2/2} = 31\,\mathrm{ps} \qquad (4)$$

$$t_{\mathrm{total,A}} = \sqrt{t_{\mathrm{det,A}}^2 + t_{\mathrm{loc,A}}^2 + t_{\mathrm{elo}}^2/2} = 51\,\mathrm{ps} \quad .$$

The resolution of the time-structure measurement with detector A or B can be calculated according to

$$t_{\mathrm{resol,B}} = \sqrt{t_{\mathrm{det,B}}^2 + t_{\mathrm{elo}}^2 + t_{\mathrm{ref}}^2} \approx 35\,\mathrm{ps} \qquad (5)$$

$$t_{\mathrm{resol,A}} = \sqrt{t_{\mathrm{det,A}}^2 + t_{\mathrm{loc,A}}^2 + t_{\mathrm{elo}}^2 + t_{\mathrm{ref}}^2} \approx 53\,\mathrm{ps}$$

with t_{ref}, the jitter of the RF-reference signal, assumed to be negligible.

Similarly, the width t_{TS} of a time spectrum measured according to Fig. 2, mode I or II is separable as

$$t_{\mathrm{TS}}^2 = t_{\mathrm{bunch}}^2 + t_{\mathrm{resol}}^2 \quad . \qquad (6a)$$

The bunch length t_{bunch} can be derived by Eq. (6a) from the measured t_{TS} and known t_{resol} (6b). Alternatively, t_{resol} can be deduced from the measured t_{TS} and the known t_{bunch} (6c).

Short bunch lengths measured according to Eq. (6b) with detectors A and B agree well, thereby corroborating the above derived values of time resolution.

Fig. 4 compares the derived time resolution, according to Eq. (4), to that of other experiments. Also the performance of the former set-ups of the time-structure monitor at Injector 2 is estimated from Eq. (6c) using t_{bunch} determined with the present set-up. The inferior time resolution is probably mainly due to the electronic components used at that time.

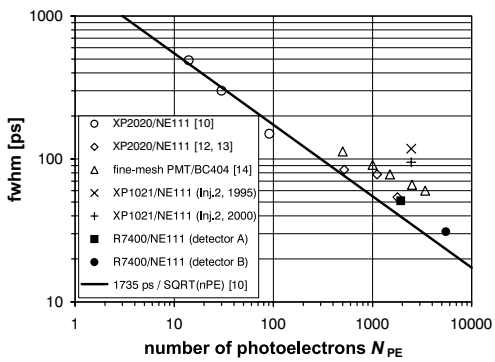

Fig. 4: Resolution of single scintillator-PMT detectors.

3.3 Bunch length and transverse width

To demonstrate the capability of the monitor, the dependency of the bunch length on proton beam current is depicted in Fig. 5 together with the transverse beam width. The bunch width is about 2/3 of the length. The bunch size decreases at lower currents with the relative dimensions approximately unchanged.

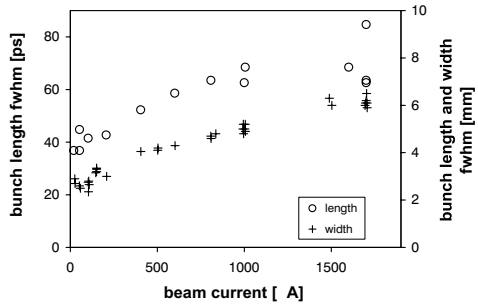

Fig. 5: Bunch length (accord. to Eq. (6b)), and width at the last turn of the Injector-2 cyclotron. (PMT 2 at position B was used. U_{PMT} in the range -700 V … -850 V.)

4 CONCLUSION

The time resolution of the time-structure monitor has been determined by a coincidence measurement. It has been improved significantly by using a set-up with enhanced light-collection efficiency, an advanced PMT (and divider circuit) and improved electronics. The detector is compact and the PMT offers an enhanced immunity to magnetic fields. Hence, a moving detector covering nearly all turns of Injector 2 seems feasible.

REFERENCES

[1] M. Olivo, "Beam diagnostic equipment for cyclotrons", Proc. 7th Int. Conf. on Cyclotrons and their Applications, Zürich (1975) p. 331
[2] W. Joho, "High intensity beam acceleration with the SIN cyclotron facility", Proc. 11th Int. Conf. on Cyclotrons and their Applications, Tokyo (1986) p. 31
[3] S. Adam, M. Humbel, "Integration of compute-bound tasks in the SIN control system", ibid. p. 418
[4] J. Stetson et al., "The commissioning of PSI Injector 2 for high intensity, high quality beams", Proc. 13th Int. Conf. on Cyclotrons and their Applications, Vancouver, Canada (1992) p. 36
[5] T. Stammbach, "Experience with high current operation of the PSI cyclotron facility", ibid. p. 28
[6] T. Stammbach et al., "The feasibility of high power cyclotrons", Nucl. Instr. & Meth. B 113 (1996) 1
[7] Manual STD-N-1, Elscint Ltd., Haifa (1973)
[8] Hamamatsu PMT R7400U data sheet TPMH1204E05 (Apr. 2000), Hamamatsu Photonics K.K.
[9] Hamamatsu PMT R7400U final test sheet (24 Oct. 2000), Hamamatsu Photonics K.K.
[10] J. Pouthas et al., "Intrinsic time resolution of detectors in a time-of-flight spectrometer", Nucl. Instr. & Meth. 145 (1977) 445
[11] P. J. Carlson, "Prospects of scintillator time-of-flight systems", Physica Scripta 23 (1981) 393
[12] M. Moszynski et al., "Timing study with R 1294 U microchannel plate photomultipliers", Nucl. Instr. & Meth. 204 (1983) 471
[13] M. Moszynski, "Prospects for new fast photomultipliers", Nucl. Instr. & Meth. A 337 (1993) 154
[14] T. Mashimo, International Center for Elementary Particle Physics, Univ. of Tokyo, private communication